www.elsevier.com/locate/talanta

A label-free electrochemical biosensor for microRNA detection based on catalytic hairpin assembly and in situ formation of molybdophosphate

Wei Cai, Shunbi Xie, Ying Tang, Yaqin Chai, Ruo Yuan, Jin Zhang

PII: S0039-9140(16)30842-6
DOI: http://dx.doi.org/10.1016/j.talanta.2016.10.086
Reference: TAL17006

To appear in: *Talanta*

Received date: 25 July 2016
Revised date: 12 October 2016
Accepted date: 23 October 2016

Cite this article as: Wei Cai, Shunbi Xie, Ying Tang, Yaqin Chai, Ruo Yuan and Jin Zhang, A label-free electrochemical biosensor for microRNA detection based on catalytic hairpin assembly and in situ formation of molybdophosphate *Talanta,* http://dx.doi.org/10.1016/j.talanta.2016.10.086

A label-free electrochemical biosensor for microRNA detection based on catalytic hairpin assembly and *in situ* formation of molybdophosphate

Wei Cai[a], Shunbi Xie[a,b], Ying Tang[b], Yaqin Chai[a], Ruo Yuan[a*], Jin Zhang[a,b*]

[a]*Education Ministry Key Laboratory on Luminescence and Real-Time Analysis, College of Chemistry and Chemical Engineering, Southwest University, Chongqing 400715, PR China*

[b]*Chongqing Key Laboratory of Environmental Materials & Remediation Technologies (Chongqing University of Arts and Sciences), Chongqing 400715, PR China*

yuanruo@swu.edu.cn

Zhangjin@cqwu.edu.cn

[*]Corresponding author. Tel.: +86 23 68252277; fax: +86 23 68253172

Abstract

A label-free electrochemical biosensor for sensitive detection of miRNA-155 was presented by coupling enzyme-catalyzed *in situ* generation of electronic mediator for signal introduction with catalytic hairpin assembly (CHA) induced target recycling amplification strategy. In this work, alkaline phosphatase (ALP) was adopted to hydrolyze inactive substrate 1-naphthyl phosphate (NPP) to produce phosphate ion (PO_4^{3-}), which could further react with acidic molybdate to form abundant molybdophosphate anion ($PMo_{12}O_{40}^{3-}$) on the surface of electrode. The produced

$PMo_{12}O_{40}^{3-}$ could directly generate a strong and stable electrochemical signal for quantitative detection of targets. In addition, CHA induced the cyclic reuse of the target was also employed as an effective strategy for improving the sensitivity of biosensor. This electrochemical method for miRNA-155 detection had achieved a good linear relationship ranging from 10 fM to 1 nM with a detection limit of 1.64 fM. With this assay successfully applied in tumor cell lysates, it holds great potential for early cancer diagnosis by employing miRNA as the effective biomarker.

Graphical abstract

Here we have constructed a label-free electrochemical biosensor for sensitive detection miRNA by coupling catalytic hairpin assembly (CHA) and enzyme-catalyzed *in situ* generation of molybdophosphate ($PMo_{12}O_{40}^{3-}$).	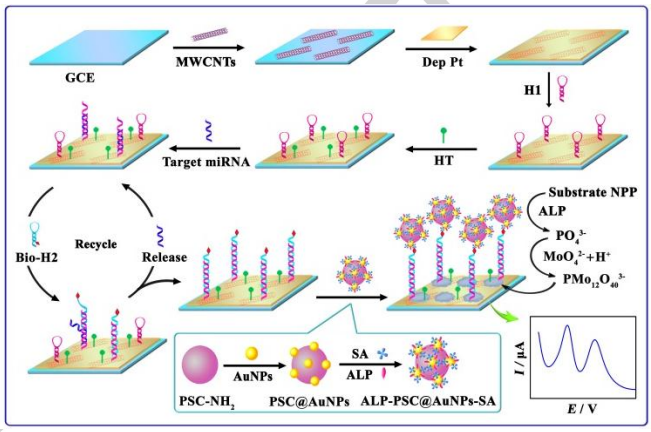

Keywords: miRNA, alkaline phosphatase, molybdophosphate, catalytic hairpin assembly

1. Introduction

MicroRNAs (miRNAs) are small non-coding RNAs that play a critical role in regulating gene expression by inhibiting target mRNA translation or degradation

(Shenouda and Alahari, 2009; Zeng et al., 2003; Di Leva and Croce, 2013; Lu and Tsourkas, 2009). Considerable researches revealed that miRNAs were associated with the pathogenesis of many human diseases, such as cancers (Iorio et al., 2005; Volinia et al., 2006), cardiovascular diseases (Quiat and Olson, 2013; van Rooij and Olson, 2012), autoimmune diseases (O'Connell et al., 2010; Leng et al., 2011), and lymphocytic leukemia (Marcucci et al., 2013). These phenomena made miRNAs serve as one of promising biomarkers for diseases diagnosis and treatment (van Rooij et al., 2012; Wang et al., 2014). However, the intrinsic characteristics of miRNAs imposed great challenge for high sensitive quantification by using traditional methods, such as reverse transcriptase polymerase chain reaction (RT-PCR) (Marabita et al., 2015), microarrays (Pai et al., 2016), and northern blotting (Pall et al., 2007). Although these approaches were usually used for miRNAs profiling, they still possess many limitations including expensive reagents, complex process and sample-consuming (Lee et al., 2016). Hence, it is desirable to develop high sensitivity and specificity together with simplicity strategy for the optimized measurement of miRNAs.

In order to achieve this goal, it is very necessary to choose a predominant analytical technique first. The electrochemical method has received great attention owning to its advantages of low cost, simplicity, rapid detection and good sensitivity (Cheng et al., 2015; Xiong et al., 2015). However, to obtain an amperometric signal, the labeling of redox mediator is usually required in a typical electrochemical method, which may inevitably increase the complexity of the operation and analytical time or

even pollute the samples. A promising approach to overcome these limitations is *in situ* generation of redox mediator to design a label-free electrochemical biosensor. In recent years, a lot of studies which based on ALP catalytic NPP to produce NP for electrochemical signal generation have been reported (Liu et al., 2016; Moreno-Guzman et al., 2012; Wu et al. 2012; Yang et al., 2015). However, the produced NP should diffuse to the surface of the electrode for further oxidation which could undoubtedly weak the electrical signal and decrease the sensitivity. In our previous work, we had proposed an electrochemical strategy based on *in situ* generation of molybdophosphate ($PMo_{12}O_{40}^{3-}$) as a redox mediator by tracing PO_4^{3-} generated during loop mediated isothermal amplification (Xie et al., 2015). This assay provided us a perspective direction for miRNAs detection by taking advantage of the byproduct. Furthermore, PO_4^{3-} as the byproduct of alkaline phosphatase (ALP) catalyzed the 1-naphthyl phosphate (NPP) to generate $PMo_{12}O_{40}^{3-}$ for miRNA detection has not been reported yet.

Currently, nucleus acid amplification techniques have become a versatile and powerful tool for signal amplification, because it could greatly enhance the sensitivity by amplifying the target sequences and strengthening the responsive signals. Therefore, electrochemical methods coupling with nucleus acid amplification strategies, for instance, hybridization chain reaction (HCR) (Hou et al., 2015; Zhao et al., 2015), rolling circle amplification (RCA) (Deng et al., 2014; Zhu et al., 2015), strand displacement amplification (SDA) (Chen et al., 2015; Zhang et al., 2016) and catalytic hairpin assembly (CHA) (Yu et al., 2016; Zhuang et al., 2014), have been

widely used in the construction of biosensors. Among them, CHA has attracted particular attention, because CHA as an enzyme-free amplification strategy can not only effectively amplify the signal, but also greatly reduce the costs and simplify the detection conditions.

Herein, we fabricated a highly sensitive electrochemical biosensor based on the PO_4^{3-} induced *in situ* formation of $PMo_{12}O_{40}^{3-}$ as the electronic mediator for miRNA-155 detection. In this work, gold nanoparticles-modified polystyrene magnetic microspheres (PSC@AuNPs) were used for immobilizing ALP and streptavidin (SA) to form ALP-PSC@AuNPs-SA bioconjugates as signal tracing probe. Platinum nanoparticles were deposited on the surface of carboxyl-functionalized MWCNTs modified electrode to capture hairpin probe (H1). Target miRNA-155 could hybridize with H1 to open its hairpin structure and expose the concealed sequence for further complementary to the biotinylated H2 (bio-H2). In the presence of bio-H2, the target hybridized with H1 was displaced from the duplex structure of H1-target. The released target was available for the next hybridization process, which resulted in a large number of bio-H2/H1 duplex left on the electrode after the cyclic amplification process. Subsequently, amounts of ALP-PSC@AuNPs-SA bioconjugates were immobilized on the modified electrode *via* the specific recognition between biotin and SA. With the introduction of NPP, ALP could effectively hydrolyze the substrate to produce PO_4^{3-}. Then, the produced PO_4^{3-} further reacted with acidic molybdate to *in situ* form $PMo_{12}O_{40}^{3-}$, which could be steadily attached to the surface of the MWCNTs-modified electrode to serve as the

electronic mediator. By taking advantage of the reversible multi-electron of the adherent $PMo_{12}O_{40}^{3-}$ on the electrode surface, the content of the target can be easily analyzed. The detection principle of the proposed biosensor was shown in scheme 1.

2. Experiment

2.1 Materials and reagents

Sodium citrate ($C_6H_5Na_3O_7 \cdot 2H_2O$), streptavidin (SA), hexanethiol (96%, HT), gold chloride ($HAuCl_4$) and chloroplatinic acid (H_2PtCl_6) were purchased from Sigma-Aldrich (St, Louis, MO, U.S.A). 1-naphthyl phosphate (NPP) was perchased from Jiang Lai Bio. Co. Ltd (Shanghai, China). Amine-modified polystyrene magnetic microspheres (PSC-NH_2) were provided by Tianjin BaseLine ChromTech Research Centre (Tianjin, China). Multiwalled carbon nanotubes (MWCNTs, >95% purity) were from Chengdu Organic Chemicals Co. Ltd. (Chengdu, China). Alkaline phosphatase (ALP, 1000 unit) was purchased from Beijing biomars-technology Co., Ltd (Beijing, China). The buffer solutions employed in this study were as follows: 20 mM Tris-HCl buffer (pH 7.4) containing 140 mM NaCl, 5 mM KCl, 1 mM $CaCl_2$ and 1 mM $MgCl_2$ was used as a binding buffer solution. 5 × TBE buffer: 445 mM Tris base, 445 mM boric acid, 10 mM EDTA (pH 8.0). Sulfuric acid (H_2SO_4, 0.25 M) was used as the supporting electrolyte. Ultrapure water (18 MΩ·cm) was employed throughout the study.

All DNA and miRNA sequences were provided by Sangon biotechnology (Shanghai, China) and were listed in Table S1.

2.2 Apparatus and measurements

The morphology of nanomaterial was analyzed by scanning electrode microscope (SEM, S-4800, Hitachi, Japan) and transmission electron microscope (TEM, JEM-1200EX, Japan). The pH measurement was performed with a pH meter (PHS-3C, Shanghai Leici Instrument Company, Ltd., China). All electrochemical measurements, including cyclic voltammetry (CV) and differential pulse voltammetry (DPV) were carried out on a CHI 660E electrochemical workstation (Shanghai Chenhua instrument, China) with a conventional three-electrode system: a modified glass carbon electrode (GCE, Φ = 4 mm) as working electrode, a platinum wire as counter electrode, and a saturated calomel electrode as reference electrode.

2.3 Carboxylation of MWCNTs

The carboxyl-functionalized MWCNTs were prepared according to the reference with some modification (Li et al., 2015). Briefly, 0.5 g MWCNTs were treated with 40 mL of H_2SO_4/HNO_3 (1 : 3 *V*/*V*) solution and refluxed for 2 h at 100 °C. Then, the reaction mixture was centrifuged and washed with ultrapure water until the pH reached 7.0, and then dried in a vacuum oven at 100 °C. Ultimately, 1.5 mg of carboxylated MWCNTs were ultrasonically dispersed in 2 mL ultrapure water to give a homogeneous solution for further use.

2.4 Preparation of ALP-PSC@AuNPs-SA bioconjugates

Gold nanoparticles (AuNPs) were firstly synthesized by sodium citrate reduction of $HAuCl_4$ according to the literature (Liu et al., 2014), then 0.5 mL (5 mg·mL^{-1}) of

aminated-PSC magnetic microspheres (PSC-NH_2) solution was isolated by magnet and washed with ultrapure water three times. Thereafter, 3 mL synthesized AuNPs were transferred into the PSC-NH_2 and stored for 1 h to obtain a homogeneous solution. Subsequently, the obtained PSC@AuNPs nanocomposites were collected with a magnet and dispersed again in 1 mL Tris-HCl (pH 7.4) to obtain a homogeneous solution. And then, 0.3 mL Tris-HCl (pH 7.4) containing ALP and SA at a 50 : 1 (ALP : SA) molar ratio were transferred into the prepared PSC@AuNPs solution and incubated for 12 h at 4 °C under 180 rpm rotation. As a result, numerous species of ALP and SA were immobilized on the surface of PSC@AuNPs nanocomposites *via* the strong Au-N affinity to obtain the ALP-PSC@AuNPs-SA bioconjugates.

2.5 Fabrication of the electrochemical biosensor

Prior to use, all the hairpin oligonucleotides were annealed at 95 °C for 5 min and then slowly cooled to room temperature. The GCE was initially polished with 0.3 and 0.05 μm alumina powder and rinsed throughly with ultrapure water. After sonication with ethanol and ultrapure water, the GCE was coated with 10 μL dispersed MWCNTs (0.75 mg·mL^{-1}) and allowed to dry under vacuum at 37 °C. Subsequently, the electrode was soaked in H_2PtCl_6 solution (1% *w*/*w*) for electrodeposition under the potential of -0.25 V for 40 s to obtain a PtNPs layer. Afterward, 15 μL of amino-modified H1 (2 μM) was dropped on the surface of PtNPs/MWCNTs modified electrode and incubated for 12 h at room temperature to achieve the attachment of amine-modified H1 onto the electrode surface. After that,

the modified electrode was washed with ultrapure water to remove the unbounded H1 on the surface. To prevent nonspecific adsorption, the electrode was blocked with 10 μL of HT (1.0 mM) for 40 min. After rinsing with ultrapure water, a mixture containing 15 μL biotinylated H2 (2 μM) and 10 μL different concentrations of target miRNA was incubated on the modified electrode for 2 h at 37 °C. Finally, the electrode was washed with ultrapure water and incubated with 10 μL of ALP-PSC@AuNPs-SA bioconjugates for 40 min at room temperature. As a result, the ALP-PSC@AuNPs-SA bioconjugates could be successfully immobilized on the electrode through the specific and sensitive recognition between biotin and SA. Finally, the proposed biosensor was fabricated for electrochemical measurement.

2.6 Electrochemical measurement

The prepared biosensor was incubated with 10 μL of 8 $mg \cdot mL^{-1}$ NPP at room temperature for 8 min. Subsequently, 10 μL of 50 mM Na_2MoO_4 and 2 μL of 0.5 M H_2SO_4 were dropped on the biosensor for 8 min. After that, the electrode was washed with ultrapure water. DPV were performed in 2 mL of 0.25 M H_2SO_4 with 0.05 V modulation amplitude, 0.05 s pulse width, 0.0167 s sample width and the potential range was from -0.05 V to 0.6 V.

2.7 Polyacrylamide gel electrophoresis

To carry out the polyacrylamide gel electrophoresis, four samples were prepared: 4 μM H1, 4 μM H2, a mixture of H1 incubated with H2 for 2 h at 37 °C without and with 10 μM miRNA-155, respectively. The samples were loaded into the notches of the freshly prepared polyacrylamide gel (16%), and electrophoresis was run at 120 V

for 120 min in 1 × TBE buffer. After that, the gel was dyed with ethidium bromide (EB) and visualized under UV light. Finally, the electrophoresis image was obtained by a digital camera.

3. Results and discussion

3.1 Investigation of the CHA via gel electrophoresis

The gel electrophoresis was performed to analyze the feasibility of CHA amplification strategy in this study. Lanes 1, 2, 3, and 4 were loaded with H1 (4 μM), H2 (4 μM), the mixture of H1 (4 μM) and H2 (4 μM), and the CHA amplification products (containing 10 μM miRNA-155, 4 μM H1 and 4 μM H2), respectively. As shown in Figure S1, the lanes 1 and 2 exhibited a clearly single band. The lane loaded with the mixture of H1 and H2 showed obvious distinct dual-band (lane 3), consisting of band matched with H1 and H2, which indicated that no reaction occurred in absence of miRNA-155. Instead, the bright single band in lane 4 showed successful formation of H1-H2 duplex.

3.2 Characterizations of different nanomaterials

The morphology and size of the MWCNTs and AuNPs were characterized by scanning electron microscope (SEM) and transmission electron microscope (TEM), respectively. The typical SEM image of MWCNTs was displayed in Figure S2A. The short tube structure suggested that the MWCNTs were successfully prepared. As seen from Figure S2B, the TEM image of the AuNPs exhibited uniform size with an average diameter about 16 nm, which suggested the successful preparation of AuNPs.

3.3 Electrochemical characterization of the biosensor

The stepwise fabrication process of the proposed biosensor was characterized by cyclic voltammetry in 2 mL of 5 mM $Fe(CN)_6^{3-/4-}$ solution containing 0.1 M KCl, scanning from -0.2 V to 0.6 V at a scan rate of 100 mV/s. As shown in Figure 1A, the bare GCE exhibited a well-defined redox peak of $[Fe(CN)_6]^{3-/4-}$ (curve a). When the MWCNTs were decorated on the electrode, a sharply increased peak current was obtained owing to the excellent electron transfer ability of the MWCNTs (curve b). With the PtNPs deposited on the surface of the electrode, the peak current was further increased because the PtNPs could facilitate the electron transfer (curve c). Nevertheless, the peak current was decreased with the assembling of H1 onto the modified electrode, which was ascribed to the steric hindrance and electrostatic repulsion of the oligonucleotides to $[Fe(CN)_6]^{3-/4-}$ (curve d). When the nonconductive HT was employed to block the nonspecific sites, the peak current was decreased again (curve e). After the mixture of H2 and target was incubated, the peak current was continuously decreased because the amplification process of CHA produced a large number of dsDNA (curve f). As a result, the electron transfer process of $[Fe(CN)_6]^{3-/4-}$ was hindered by the negatively charged phosphate backbone of dsDNA. With the introduction of ALP-PSC@AuNPs-SA bioconjugates, the peak current was slightly increased (curve g), which was mainly attributed to the good electronic conductivity of PSC@AuNPs. This increase suggested that ALP-PSC@AuNPs-SA bioconjugates were successfully immobilized on the electrode.

3.4 Characterization and validation of the $PMo_{12}O_{40}^{3-}$

In order to validate that the current signal was produced by the $PMo_{12}O_{40}^{3-}$, the current signal of the electrode before and after forming $PMo_{12}O_{40}^{3-}$ was investigated. As shown in Figure 1B, no obvious redox peak was found at the ALP-PSC@AuNPs-SA bioconjugates modified electrode (curve a). However, two pairs of redox peaks (at 0.13 V and 0.32 V) could be clearly observed when the ALP-PSC@AuNPs-SA bioconjugates modified electrode was incubated with NPP, Na_2MoO_4 and H_2SO_4 (curve b). This result reflected that the electrochemical signal was generated from $PMo_{12}O_{40}^{3-}$ (Talarico et al., 2015). The two pairs of redox peaks were relative to two successive steps of electron transfer process between $PMo_{12}O_{40}^{3-}$ and $H_2PMo_2^{V}Mo_{10}^{VI}O_{40}^{3-}$ (see Figure S3), which is in agreement with previous reports (Xie et al., 2015; Lin and Jiang, 2006).

3.5 Optimization of the experimental conditions

In order to achieve an optimal analytical performance of the detection system, the important experiment parameters including the supporting electrolyte concentration of H_2SO_4, the concentration and incubation time of substrate NPP, and the deposition time of $PMo_{12}O_{40}^{3-}$ were investigated. Considering that the response current was dependent on the concentration of supporting electrolyte, the influence of different concentration of H_2SO_4 was investigated. As shown in Figure S4A, the highest electrochemical signal was observed at the concentration of 0.25 M at the

potential of 0.32 V. Therefore, 0.25 M H_2SO_4 was selected as the supporting electrolyte in the whole experiments.

The electrochemical signal was produced by $PMo_{12}O_{40}^{3-}$, which mainly derived from the enzymatic hydrolysis of NPP by ALP. Thus, the concentration of NPP had a great influence in the electrochemical signal. The relationship between the concentration of NPP and current response was presented in Figure S4B. The current signal increased along with the increase of NPP concentration from 2 $mg \cdot mL^{-1}$ to 8 $mg \cdot mL^{-1}$ but decreased remarkably with the concentration increase continuously. Thus, the NPP concentration of 8 $mg \cdot mL^{-1}$ was employed as the optimized concentration of the NPP in this work.

The inactive substrate NPP was catalyzed by ALP to generate PO_4^{3-}, which was a time-dependent process. Thus, we further investigated the incubation time of NPP on the electrode surface. As shown in Figure S4C, the electrochemical response increased quickly at first and then leveled off after 8 min. Thus, we used 8 min as the optimum catalysis time in the following experiment. The deposition time of $PMo_{12}O_{40}^{3-}$ was also the one of important factors. As displayed in Figure S4D, The current signal gradually increased with the prolongation of deposition time, which was due to that more $PMo_{12}O_{40}^{3-}$ have been accumulated on the surface of electrode. However, the current signal increased slightly when the deposition time increased over 8 min. Thus, 8 min was adopted as the deposition time in the following work.

3.6 Contribution of ALP and PSC on signal amplification

To evaluate the effect of ALP on the signal amplification of this approach, the electrochemical biosensor without and with ALP was investigated. The effect of amplification was evaluated by the peak current change (ΔI). As shown in Figure 2A, in the absence of ALP, a small electrochemical oxidation signal was observed at 0.32 V (curve a). In the presence of ALP, the ALP-PSC@AuNPs-SA bioconjugates could efficiently catalyze NPP to produce amounts of PO_4^{3-}, resulting in an obvious increase of the current response (curve b). The peak current change ΔI was 172.8 μA. This increased current response indicated that the ALP played a crucial role in the signal amplification strategy.

We also investigated the performance of the biosensor with different nanocarriers. As shown in Figure 2B, when the proposed biosensor was modified with ALP-PSC@AuNPs-SA, a remarkable increase in the current response was found (ΔI = 81.1 μA) compared with the biosensor modified with ALP-AuNPs-SA. The reason for this phenomenon was that the larger effective surface area of PSC@AuNPs nanoparticles could enormously increase the loading amount of ALP for signal amplification. Thus, the current signal of the electrochemical biosensor could be significantly improved.

3.7 Calibration curves of the electrochemical biosensor

The sensitivity and dynamic range of the proposed biosensor was monitored by incubation with different concentrations of miRNA-155 under the optimal conditions. As we could see from Figure 3A, the peak current increased with increasing

concentration of miRNA-155. Figure 3B illustrated that the current response of calibration plots exhibited a good linear relationship between the peak currents (at the potential of 0.32 V) and the logarithm of the concentration of miRNA-155 in the range from 10 fM to 1 nM. The linear regression equation was obtained as I (μA) = 324.83 + 32.09 lgc_{miRNA} (nM) with the correlation coefficient of r = 0.9986. And the detection limit was evaluated to be 1.64 fM at a signal-to-noise ratio of 3σ (where σ is the standard deviation of a blank sample, n = 11). In addition, the performance of our biosensor was also compared with other biosensors which were summarized in Table 2. The electrochemical biosensor designed in this study exhibited higher sensitivity and wider linear response range than other reported works.

3.7 Selectivity, stability, and reproducibility of the proposed biosensor

To validate the selectivity of the electrochemical biosensor, four types of miRNA including miRNA-21, miRNA-141, miRNA-199A and sRNA were analyzed under the same conditions at the concentrations of 20 pM. As shown in Figure 4A, the peak currents of miRNA-21, miRNA-141, miRNA-199A, and sRNA (20 pM) showed no significant change compared with the blank analyte, whereas a significantly higher electrochemical signal was obtained when the biosensor incubated with 2 pM miRNA-155. Meanwhile, the coexistence of the above four interferences (20 pM of miRNA-21, miRNA-141, miRNA-199A and sRNA) with 2 pM miRNA-155 did not cause an obvious change compared with the miRNA-155 alone. These results indicated the outstanding selectivity of the developed biosensor for miRNA-155

detection.

The reproducibility was studied by analysis of five different electrodes in the same batch. As shown in Figure 4B, a coefficient of variation of 2.46% was found, illustrating the acceptable reproducibility of the electrochemical biosensor. The stability was evaluated by the CV response under continuous cyclic potential scans for 100 cycles. As shown in Figure 4C, a 5.37% decrease of initial response was obtained, indicating an excellent stability of the proposed biosensor due to the strong chemisorption between the MWCNTs and $PMo_{12}O_{40}^{3-}$ (Wei et al., 2014).

3.8 Application of the electrochemical biosensor in tumor cell lysates

To monitor whether this assay was reliable in real samples, we analyzed miRNA-155 in the lysates derived from two cancerous cell lines, Hela (cervical cancer cells) and MDA-MB-231 (human breast cancer cell lines). As shown in Figure 5, when the lysate of Hela cells (100 cells) was incubated on the electrochemical biosensor, there was only a slight increase in the current response compared to the blank analyte. With the Hela cells increase to 10^5 cells, there was an insignificant increase in the current signal, suggesting a low expression of miRNA-155 in Hela cells. In contrast, when the biosensor was incubated with the lysates of 100 MDA-MB-231 cells, an obvious increase could be found. With the elevating of MDA-MB-231 cell numbers, a significant increase of the current response was obtained. This phenomenon indicated that miRNA-155 showed a high expression in MDA-MB-231 cells. These results demonstrated that the miRNA-155 was

overexpressed in MDA-MB-231 cells but not in Hela cells, which was consistent with previous reports (Lu et al., 2009; Jiang et al., 2010; Zhou et al., 2016). Therefore, this study provided a potential assay to monitor miRNA in cancer cells.

4 Conclusions

In summary, this work constructed a highly sensitive electrochemical biosensor for miRNA-155 detection based on *in situ* formation of $PMo_{12}O_{40}^{3-}$ for signal introduction. Incorporation of the CHA strategy and PSC@AuNPs nanocomposites could significantly enhance the sensitivity of the biosensor. Compared with traditional electrochemical methods, this approach utilized the byproduct of ALP-catalyzed reaction to *in situ* generate electronic mediator for direct quantitative analysis of targets, which avoided the fussy labeling steps and complicated operation processes. Moreover, the produced $PMo_{12}O_{40}^{3-}$ displayed a strong chemisorption on carbon materials, which was beneficial to produce a stable electrochemical response signal. Importantly, this approach could be successfully applied in real samples, which provided the potential for miRNA detection in clinical diagnostics.

Acknowledgements

This work was financially supported by the National Natural Science Foundation (NNSF) of China (21575116, 21275119, 51473136), the Chongqing Science & Technology commission (cstc2015jcyjBX0126), China.

References

Cheng, F. F., He, T. T., Miao, H. T., Shi, J. J., Jiang, L. P., Zhu, J. J., 2015. ACS Appl. Mater. Interfaces 7, 2979-2985.

Chen, A. Y., Gui, G. F., Zhuo, Y., Chai, Y. Q., Xiang, Y., Yuan, R., 2015. Anal. Chem. 87, 6328-6334.

Deng, R. J., Tang, L. H., Tian, Q. Q., Wang, Y., Lin, L., Li, J. H., 2014. Angew. Chem. Int. Ed. 53, 2389-2393.

Di Leva, G., Croce, C. M., 2013. Curr. Opin. Genet. De. 23, 3-11.

Hao. N., Dai, P. P., Yu, T., Xu, J. J., Chen, H. Y., 2015. Chem. Commun. 51, 13504-13507.

Hou, T., Li, W., Liu, X. L., Li, F., 2015. Anal. Chem. 87, 11368-11374.

Iorio, M. V., Ferracin, M., Liu, C. G., Veronese, A., Spizzo, R., Sabbioni, S., Magri, E., Pedriali, M., Fabbri, M., Campiglio, M., Menard, S., Palazzo, J. P., Rosenberg, A., Musiani, P., Volinia, S., Nenci, I., Calin, G. A., Querzoli, P., Negrini, M., Croce, C. M., 2005. Cancer Res. 65, 7065-7070.

Jiang, S., Zhang, H. W., Lu, M. H., He, X. H., Li, Y., Gu, H., Liu, M. F., Wang, E. D., 2010. Cancer Res. 70, 3119-3127.

Lee, H., Shapiro, S. J., Chapin, S. C., Doyle, P. S., 2016. Anal. Chem. 88, 3075-3081.

Leng, R. X., Pan, H. F., Qin, W. Z., Chen, G. M., Ye, D. Q., 2011. Cytokine Growth Factor Rev. 22, 141-147.

Li, J., Wang, J. J., Guo, X., Zheng, Q., Peng, J., Tang, H., Yao, S. Z., 2015. Anal. Chem. 87, 7610-7617.

Li, J. B., Lei, P. H., Ding, S. J., Zhang, Y., Yang, J. R., Cheng, Q., Yan, Y. R., 2016. Biosens. Bioelectron. 77, 435-441.

Lin, X. Q., Jiang, C. M., 2006. Anal. Sci. 22, 697-700.

Liu, M., Wang, Z. Y., Zong, S. F., Chen, H., Zhu, D., Wu, L., Hu, G. H., Cui, Y. P., 2014. ACS Appl. Mater. Interfaces 6, 7371-7379.

Liu, S. F., Wei, W. J., Sun, X. Y., Wang L., 2016. Biosens. Bioelectron. 83, 33-38.

Lu, J., Tsourkas, A., 2009. Nucleic Acids Res. 37, e100.

Lu, Y. J., Xiao, J. N., Lin, H. X., Bai, Y. L., Luo, X. B., Wang, Z. G., Yang, B. F., 2009. Nucleic Acids Res. 37, e24.

Marabita, F., de Candia, P., Torri, A., Tegner, J., Abrignani, S., Rossi, R. L., 2015. Brief. Bioinform. 17, 204-212.

Marcucci, G., Maharry, K. S., Metzeler, K. H., Volinia, S., Wu, Y. Z., Mrozek, K., Nicolet, D., Kohlschmidt, J., Whitman, S. P., Mendler, J. H., Schwind, S., Becker, H., Eisfeld, A. K., Carroll, A. J., Powell, B. L., Kolitz, J. E., Garzon, R., Caligiuri, M. A., Stone, R. M., Bloomfield, C. D., 2013. J. Clin. Oncol. 31, 2086-2093.

Moreno-Guzman, M., Ojeda, I., Villalonga, R., Gonzalez-Cortes, A., Yanez-Sedeno, P., Pingarron, Jose M., 2012. Biosens. Bioelectron. 35, 82-86.

O'Connell, R. M., Rao, D. S., Chaudhuri, A. A., Baltimore, D., 2010. Nat. Rev. Immunol. 10, 111-122.

Pall, G. S., Codony-Servat, C., Byrne, J., Ritchie, L., Hamilton, A., 2007. Nucleic Acids Res. 35, e60.

Pai, J., Hyun, S., Hyun, J. Y., Park, S. H., Kim, W. J., Bae, S. H., Kim, N. K., Yu, J., Shin, I., 2016. J. Am. Chem. Soc. 138, 857-867.

Quiat, D., Olson, E. N., 2013. J. Clin. Invest. 123, 11-18.

Shenouda, S. K., Alahari, S. K., 2009. Cancer Metast. Rev. 28, 369-378.

Talarico, D., Arduini, F., Amine, A., Moscone, D., Palleschi, G., 2015. Talanta 141, 267-272.

van Rooij, E., Olson, E. N., 2012. Nat. Rev. Drug Disco. 11, 860-872.

van Rooij, E., Purcell, A. L., Levin, A. A., 2012. Circ. Res. 110, 496-507.

Volinia, S., Calin, G. A., Liu, C. G., Ambs, S., Cimmino, A., Petrocca, F., Visone, R., Iorio, M., Roldo, C., Ferracin, M., Prueitt, R. L., Yanaihara, N., Lanza, G., Scarpa, A., Vecchione, A., Negrini, M., Harris, C. C., Croce, C. M., 2006. Proc. Natl. Acad. Sci. USA 103, 2257-2261.

Wang, X. H., Wang, H. K., Li, Y., Hafner, M., Banerjee, N. S., Tang, S., Briskin, D., Meyers, C., Chow, L. T., Xie, X., Tuschl, T., Zheng, Z. M., 2014. Proc. Natl. Acad. Sci. USA 111, 4262-4267.

Wei, T. X., Chen, Y. Y., Tu, W. W., Lan, Y. Q., Dai, Z. H., 2014. Chem. Commun. 50, 9357-9360.

Wu, H. W., Liu, S. C., Jiang, J. H., Shen, G. L., Yu, R. Q., 2012. Chem. Commun. 48, 6280-6282.

Xie, S. B., Yuan, Y. L., Chai, Y. Q., Yuan, R., 2015. Anal. Chem. 87, 10268-10274.

Xiong, E. H., Zhang, X. H., Liu, Y. Q., Zhou, J. W., Yu, P., Li, X. Y., Chen, J. H., 2015. Anal. Chem. 87, 7291-7296.

Yang, Z. H., Zhuo, Y., Yuan, R., Chai, Y. Q., 2015. ACS Appl. Mater. Interfaces 7, 10308-10315.

Yu, Y. Q., Wang, J. P., Zhao, M., Hong, L. R., Chai, Y. Q., Yuan, R., Zhuo, Y., 2016. Biosens. Bioelectron. 77, 442-450.

Yu, Y. Y., Chen, Z. G., Shi, L. J., Yang, F., Pan, J. B., Zhang, B. B., Sun, D. P., 2014. Anal. Chem. 86, 8200-8205.

Zeng, Y., Yi, R., Cullen, B. R., 2003. Proc. Natl. Acad. Sci. USA, 100, 9779-9784.

Zhang, J. P., Li, C., Zhi, X., Ramon, G. A., Liu, Y. L., Zhang, C. L., Pan, F., Cui, D. X., 2016. Anal. Chem. 88, 1294-1302.

Zhang, Y., Yan, Y. R., Chen, W. H., Cheng, W., Li, S. Q., Ding, X. J., Li, D. D., Wang, H., Ju, H. X., Ding, S. J., 2015. Biosens. Bioelectron. 68, 343-349.

Zhao, J., Hu, S. S., Cao, Y., Zhang, B., Li, G. X., 2015. Biosens. Bioelectron. 66, 327-331.

Zhou, W. J., Li, D. X., Xiong, C. Y., Yuan, R., Xiang, Y., 2016. ACS Appl. Mater. Interfaces 8, 13303-13308.

Zhu, W. Y., Su, X. P., Gao, X. Y., Dai, Z., Zou, X. Y., 2014. Biosens. Bioelectron. 53, 414-419.

Zhu, X. L., Shen, Y. L., Cao, J. P., Yin, L., Ban, F. F., Shu, Y. Q., Li, G. X., 2015. Chem. Commun. 51, 10002-10005.

Zhuang, J. Y., Lai, W. Q., Chen, G. N., Tang, D. P., 2014. Chem. Commun. 50, 2935-2938.

Scheme 1. Schematic illustration of the electrochemical biosensor based on *in situ* formation of $PMo_{12}O_{40}^{3-}$ for miRNA detection.

Figure 1. (A) CV responses of each modified step in 5 mM $[Fe(CN)_6]^{3-/4-}$ solution containing 0.1 M KCl: (a) bare GCE , (b) GCE/MWCNTs, (c) GCE/MWCNTs/PtNPs, (d) GCE/MWCNTs/PtNPs/H1, (e) blocking with HT, (f) introducing of CHA, and (g) after incubation with ALP-PSC@AuNPs-SA bioconjugates. (B) DPV responses of the proposed biosensor: before (a) and after (b) the formation of $PMo_{12}O_{40}^{3-}$, respectively.

Figure 2. (A) Comparison of the current change of the electrochemical biosensor without ALP (a) and with ALP (b); (B) DPV responses of the proposed biosensor modified with different

nanocarriers: ALP-AuNPs-SA (a), and ALP-PSC@AuNPs-SA (b).

Figure 3. (A) DPV responses of the electrochemical biosensor to different concentrations of miRNA-155 in 0.25 M H_2SO_4. (B) The calibration plots of the current response at the potential of 0.32 V *versus* the logarithm of miRNA-155 concentration.

Figure 4. (A) Selectivity of the biosensor towards different interferences: miRNA-21 (20 pM), miRNA-141 (20 pM), miRNA-199A (20 pM), sRNA (20 pM) and mixture (containing 20 pM of miRNA-21, miRNA-141, miRNA-199A, sRNA, and 2 pM miRNA-155). (B) Reproducibility of the proposed biosensor incubated with 2 pM miRNA-155 in the same batch. (C) Stability of the proposed biosensor under successive CV scans at the scan rate of 100 mV/s for 100 cycles.

Figure 5. Detection of miRNA-155 from Hela and MDA-MB-231 cell lysates.

Highlights

- Monitoring miRNA by utilizing PO_4^{3-} to *in situ* form molybdophosphate.
- Analytical performance of the biosensor is down to femtomolar level.
- Displaying excellent applicability for evaluating miRNA-155 in tumor cell lysates.

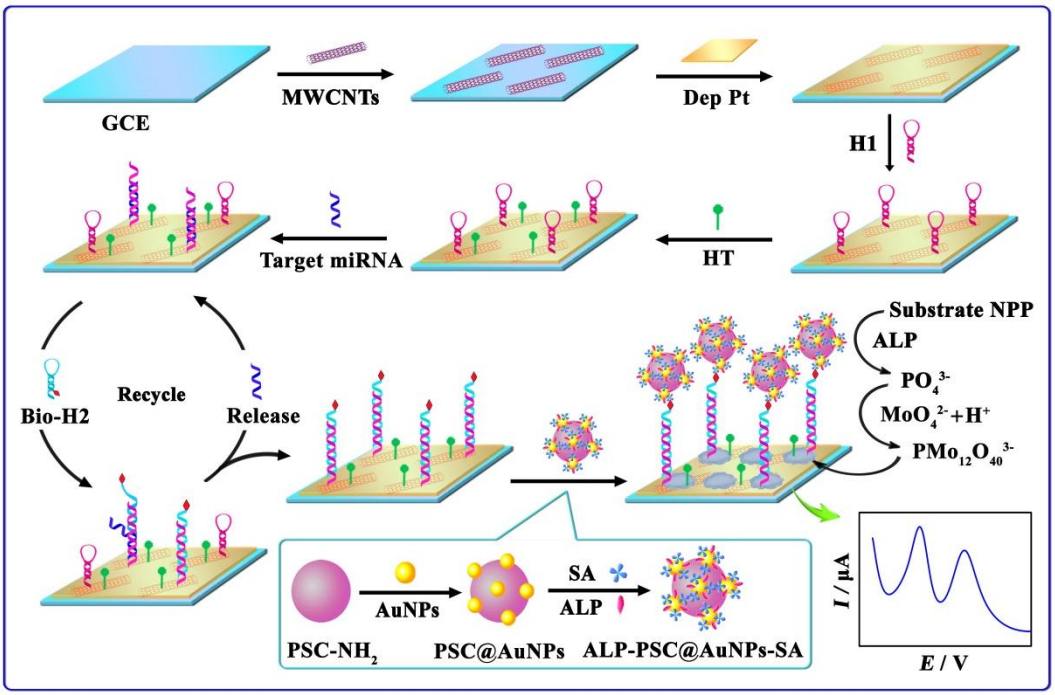

Scheme 1

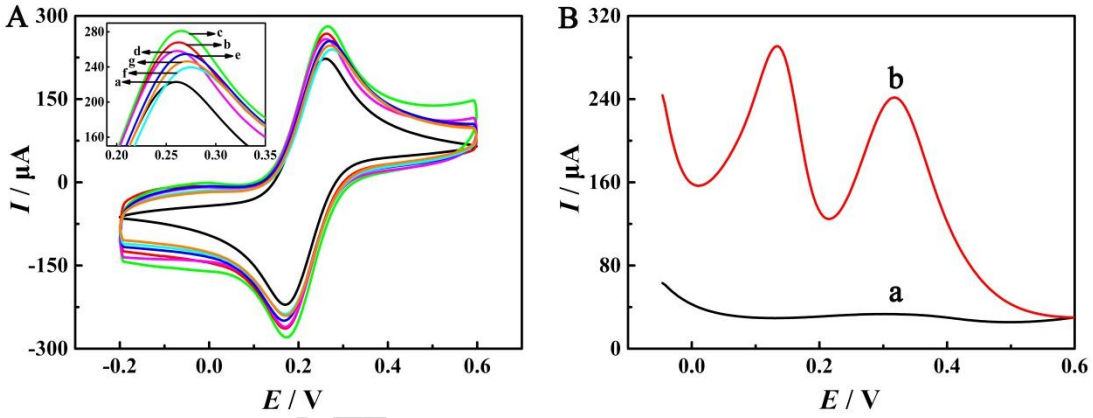

Figure 1

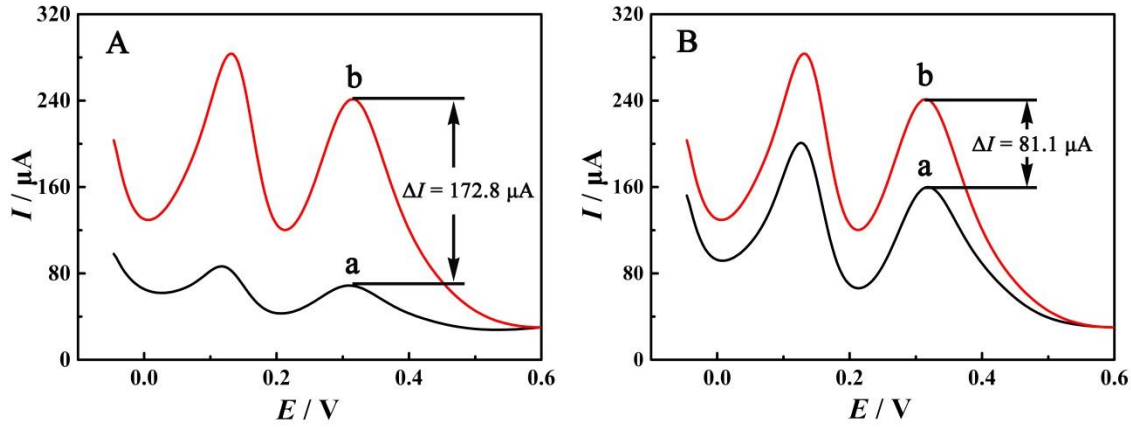

Figure 2

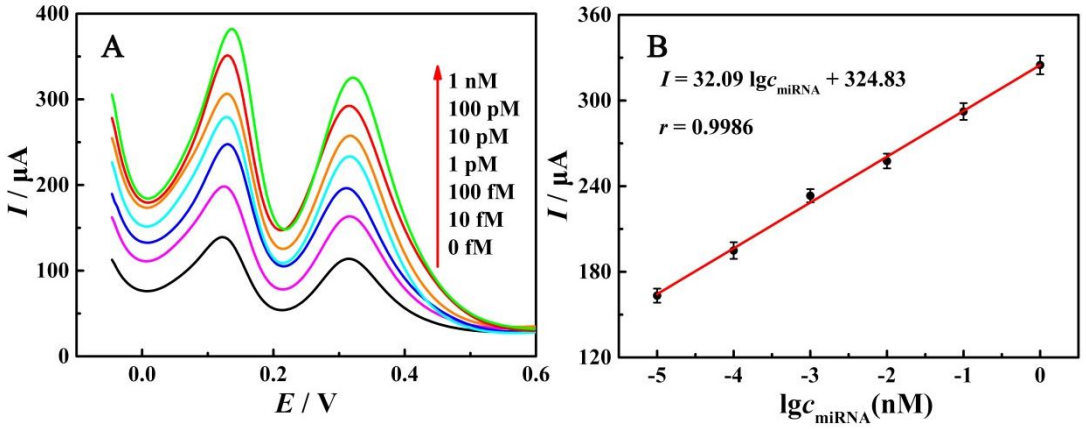

Figure 3

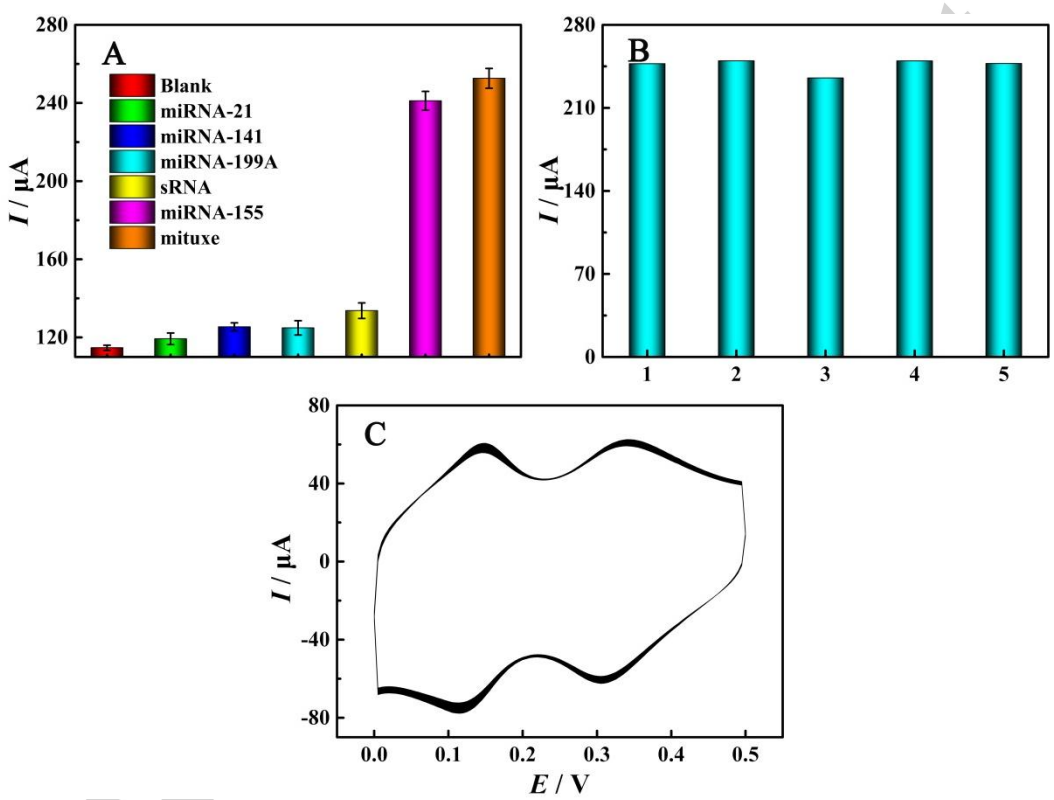

Figure 4

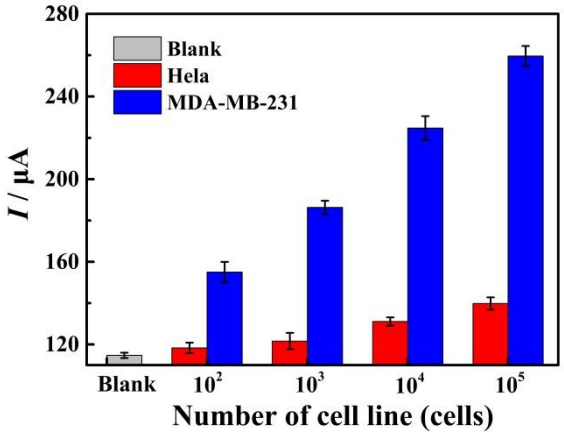

Figure 5